High-Dynamic-Range, Single-Shot Cross-Correlator Based on an Optical Pulse Replicator

Introduction

New temporal diagnostics are constantly being developed to match the evolution of optical sources and their applications. Laser systems can now generate optical intensities as high as 10^{21} W/cm^2 (Ref. 1), and short-pulse laser systems delivering energies higher than 1 kJ are currently being developed.[2] The characterization of high-energy laser systems is challenging because their repetition rate is usually low. Incoherent processes such as laser and parametric fluorescence can induce significant variations of the intensity from shot to shot. Large shot-to-shot variations preclude the use of averaging and scanning diagnostics. The interaction regime of an optical pulse with a target is set by the peak intensity on target, but the prepulse intensity can significantly influence the interaction. The temporal intensity of the pulse must be known over an extended temporal range (for example, hundreds of picoseconds before the main pulse) with a high dynamic range (for example, eight orders of magnitude below the peak intensity of the pulse). These requirements are currently beyond the capabilities of single-shot optical pulse characterization techniques.[3–5]

Scanning nonlinear cross-correlators have been used for high-dynamic-range intensity measurements.[6,7] These diagnostics gate the pulse under test using an instantaneous nonlinear interaction with another optical pulse. The representation of the intensity of the pulse under test is obtained by scanning the delay between the interacting pulses. The scanning range can be very large since it is limited only by the ability to scan the relative delay between optical pulses. The dynamic range is set for each time slot by adjusting the signal level on the detector. For example, a combination of variable attenuation at the input of the diagnostic and variable gain at the detection stage may be used to adapt the signal level before detection. These diagnostics are fundamentally multi-shot devices.

Single-shot cross-correlators using time-to-space encoding have been demonstrated.[8,9] In these devices, nonlinear interaction in an appropriate arrangement maps the temporal intensity of the pulse under test onto a spatial-intensity distribution, which can be measured in a single shot. If the pulse-front tilt from a diffraction grating is used,[9] a large temporal coverage can be obtained. Since photodetectors and analog-to-digital converters are usually limited to a dynamic range of the order of 1000, the different temporal slices of the gated signal were selectively attenuated in Ref. 9 to make it possible to measure a 60-dB dynamic range using a low-dynamic-range detector. In practice, custom, continuous, spatially varying, neutral-density filters would be required to adjust the sensitivity of the device.

This article demonstrates a single-shot cross-correlator based on an optical pulse replicator. The replicator generates a discrete sequence of sampling pulses that are cross-correlated with the source under test in a nonlinear crystal. Advantages of this technique include (1) long temporal ranges, (2) sensitivity adjustments on the sampling pulses using standard neutral-density filters, and (3) constant temporal resolution over the full temporal range of the diagnostic. The remaining three sections describe the design of the cross-correlator, review various experimental results, and present conclusions.

Design of a Single-Shot, High-Dynamic-Range Cross-Correlator Based on a Pulse Replicator

1. General Principle

Following Fig. 114.36(a), the single-shot, high-dynamic-range cross-correlator correlates the pulse under test with a sequence of sampling pulses in a nonlinear crystal, and the spatial intensity of the resulting signal maps the temporal intensity of the input pulse. For the purpose of this explanation and demonstration, the following approximate optical frequencies apply: 1ω for the pulse under test, 2ω for the sequence of sampling pulses, and 3ω for the resulting nonlinear signal. The sampling pulses are temporally delayed and spatially displaced to ensure that the pulse under test is sampled at different times and the nonlinear signals corresponding to different times are spatially distinguishable. These pulses are generated by an optical pulse replicator (OPR) composed of a high reflector (HR) and a partial reflector (PR) appropriately aligned. This arrangement is an adjustable version of a Fabry–Perot etalon with an uncoated entrance window,[10] which has
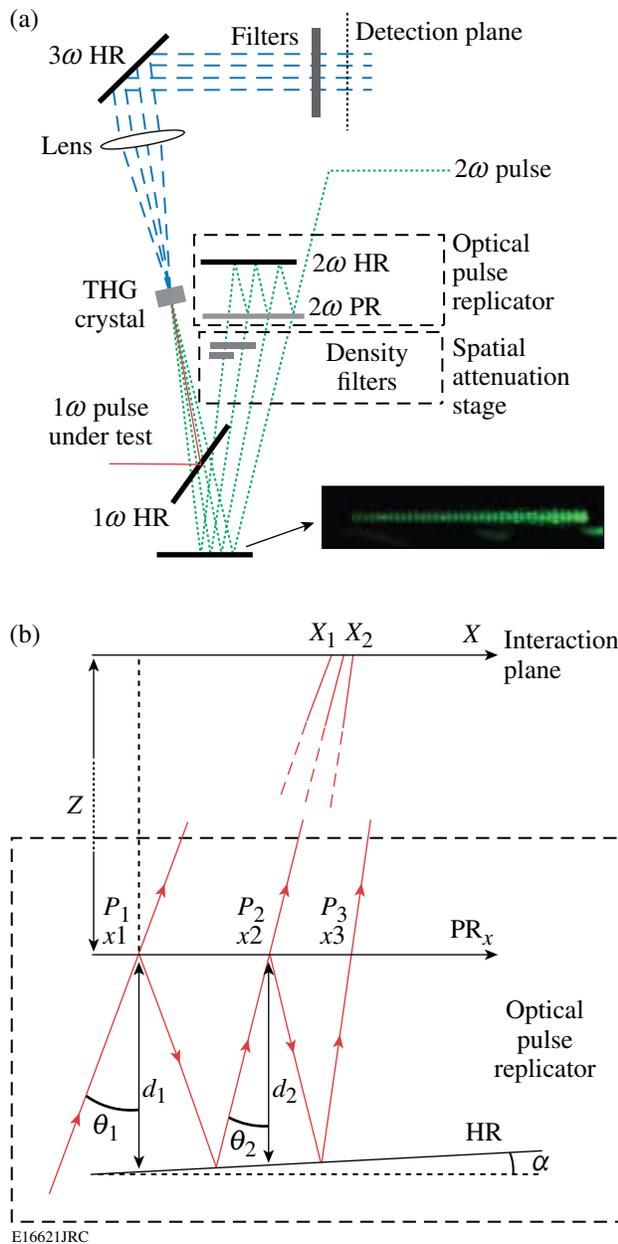
Figure 114.36

(a) Design of a single-shot cross-correlator based on the nonlinear interaction of the pulse under test with a sequence of sampling pulses from an optical pulse replicator. (b) Layout for the calculation of the spatial and temporal properties of the sequence of pulses from the optical pulse replicator. HR: high reflector; PR: partial reflector.

been used to generate discrete sequences of optical pulses.[11] In this demonstration, the pulse entering the OPR has an optical frequency of 2ω and has been obtained by doubling the input pulse under test. After the OPR, a set of neutral-density filters can selectively attenuate the sampling pulses corresponding

to high-intensity portions of the pulse under test. This allows one to balance the intensity of the nonlinear signals. The pulse under test and sampling sequence are combined in a quasi-collinear fashion and interact in a third-harmonic-generation (THG) crystal. The time-to-wave-vector encoding performed by the OPR at 2ω at the nonlinear crystal is converted into a time-to-space encoding of the 3ω signals with a lens of focal length f located a distance f away from the nonlinear crystal and the detection plane. This makes it possible to measure each individual signal corresponding to the nonlinear interaction of the pulse under test with each sampling pulse; i.e., the discrete temporal slices gated by the sequence of sampling pulses are located at discrete, spatially distinct locations of the detection plane.

2. Design and Characteristics of the Replicator

The pulse replicator is a combination of a high reflector (HR) and a partial reflector (PR) set to provide a sequence of sampling pulses after multiple reflections. Following Fig. 114.36(b), the input pulse is incident on the PR at point P_1, and part of the pulse is transmitted, generating the first sampling pulse. The remaining part of the pulse is reflected toward the HR and reflected back by the HR. The beam reflected by the HR is incident on the PR at point P_2. The pulse transmitted through the PR is the second sampling pulse, and the main part of the pulse is reflected again toward the HR to generate successive sampling pulses. For an energy E_0 at the input of the OPR, the energy of pulse n coming out of the OPR is $E_0 R^{n-1} T$, where R and T are, respectively, the intensity reflection and transmission coefficients of the partial reflector. Assuming $R = 99\%$ and a perfect high reflector, the energy of the first sampling pulse is 1% of the input pulse energy, while the energy of the 50th sampling pulse is 0.61%.

The replicator generates a sequence of sampling pulses that can be used either in the far field (i.e., the pulses are focused in the nonlinear crystal), or in a quasi near field (i.e., the pulses propagate in free space between the replicator and the nonlinear crystal). In the far-field implementation, the beams from the replicator are parallel in the near field and focused to a single point in the far field. This requires a good-quality lens with a large aperture (e.g., 2 in. for a 2-in. OPR). Care must also be taken to optimize the angular phase matching of focused beams. The overlap of multiple beams from the OPR with the pulse under test between beams might also be difficult to achieve. It was found that the sensitivity of the near-field implementation was satisfactory for the targeted application, so the near-field implementation described in the next paragraph was used.

A geometrical treatment of the near-field implementation is shown in Fig. 114.36(b). The two reflectors are set at an angle α. The existence of an optimal angle α for which all the beams from the replicator are in the same vicinity (with a tolerance associated to the beam size) at a given distance from the replicator must be proven. In practice, one of the reflectors can be set on a gimbal/kinematic mount. An interaction plane at a distance Z from the PR, where the nonlinear interaction will take place, is considered. The input beam is incident on the PR at an angle θ_1 in the point P_1 chosen as the spatial origin. The distance between the PR and the HR following a line perpendicular to the PR at point P_1 is d_1. Naming θ_n and d_n the corresponding quantities for point P_n, one can show that

$$\theta_n = \theta_{n-1} - 2\alpha \tag{1}$$

$$d_n = d_{n-1} \frac{1 - \tan(\alpha)\tan(\theta_{n-1} - 2\alpha)}{1 + \tan(\theta_{n-1})\tan(\alpha)} \tag{2}$$

$$x_n = x_{n-1} + d_{n-1} \frac{\tan(\theta_{n-1}) + \tan(\theta_{n-1} - 2\alpha)}{1 + \tan(\alpha)\tan(\theta_{n-1})}. \tag{3}$$

The sampling pulse coming out of the replicator at point P_n crosses the plane parallel to the PR at a distance Z at the coordinate $X_n = x_n + Z\tan(\theta_n)$. The corresponding optical path length L_n relative to point P_1 is the sum of the length accumulated in the replicator and the length between the PR and the interaction plane. One has the relation

$$L_n = L_{n-1} + \frac{d_{n-1}}{\left[1 + \tan(\alpha)\tan(\theta_{n-1})\right]}$$

$$\times \left[\frac{1}{\cos(\theta_{n-1})} + \frac{1}{\cos(\theta_{n-1} - 2\alpha)}\right] + \frac{Z}{\cos(\theta_n)} \tag{4}$$

with $L_1 = Z/\cos(\theta_1)$. Equations (1)–(4) allow one to calculate the position of the replicas at the interaction plane (i.e., the collection of X_n) and the delays between replicas (i.e., the delays calculated from the collection of L_n). The nonlinear crystal and the 1ω beam can be set to match the average value of the positions X_n of the sampling pulses, and the spatial performance of the OPR depends on the spreading of the X_n relative to their average value. The distance between the two reflectors sets the average delay between replicas (i.e., the sampling rate), and the temporal performance of the OPR depends on the nonuniformity of the sampling rate over the measured temporal range.

Figure 114.37 shows a simulation of the spatial characteristics of a pulse replicator with $\theta_1 = 20°$ and $Z = 1$ m. The results are plotted as a function of the sampling pulse number (between 1 and 50) and angle α. This corresponds to the situation where the distance Z is fixed in the diagnostic and the angle α is tuned. For the particular value $Z = 1$ m, the sampling pulses optimally overlap for $\alpha = 0.31$ mrad. Figure 114.37(b) displays the values of X_n for this value of α. The intersections of the sampling pulses with the reference plane are spread within 300 μm of the mean position. Such spreading will have minimal impact provided that it is small relative to the
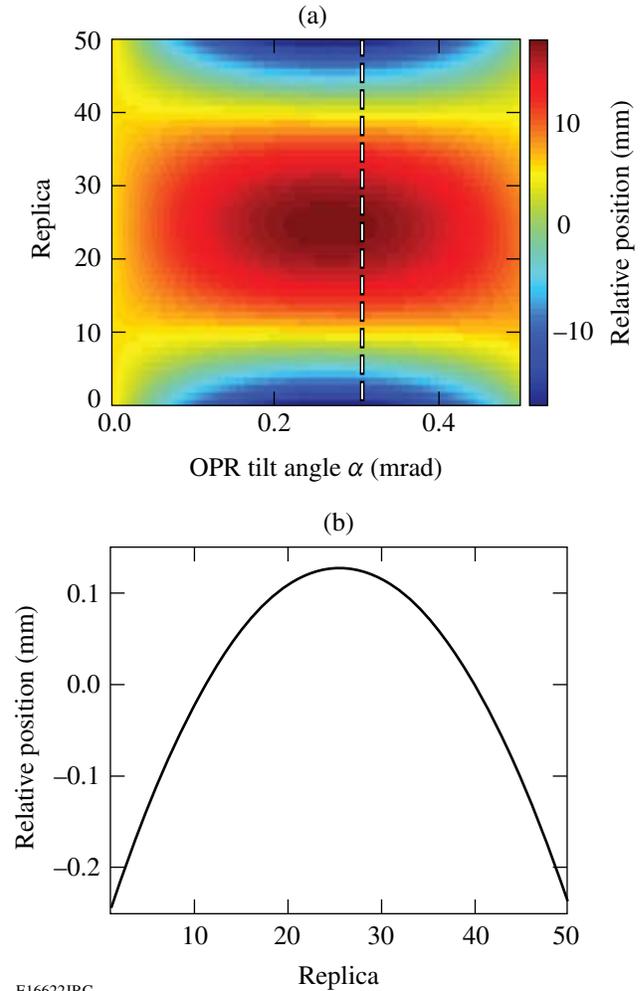
Figure 114.37
(a) Relative position (mm) of 50 replicas from the pulse replicator versus relative angle of the two reflectors of the OPR. The value of α minimizing the spread of the relative positions is indicated by a white dashed line. (b) Relative position of 50 replicas from the pulse replicator for the relative angle minimizing the standard deviation of the relative positions.

E16622JRC

size of the interacting beams. Figure 114.38(a) shows the non-uniformity of the sampling rate versus the sampling pulse number. Figure 114.38(b) displays the delay for the value of α leading to the optimal overlap plotted in Fig. 114.37(a). The average delay between replicas is 6.26 ps, and an insignificant change of the sampling rate of 0.3 ps over the 50 replicas is observed. Signal variation due to imperfect spatial overlap can be calibrated, as described in the following section, since it is a property of the diagnostic for a specific input beam size that does not depend on the temporal characteristics of the pulse.

(a)

(b)
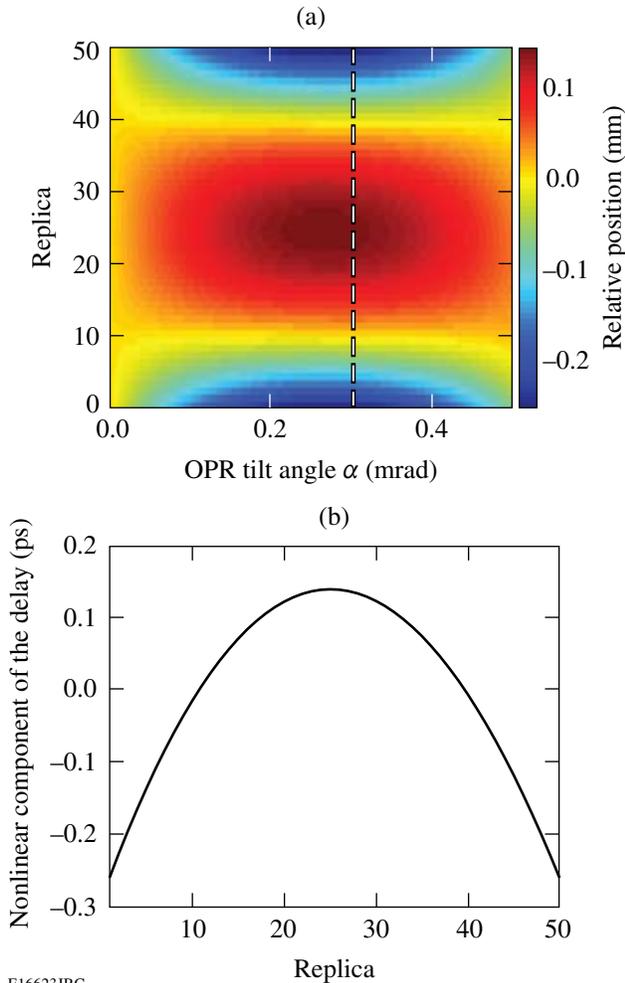
Figure 114.38

(a) Nonlinear component of the delay (ps) for 50 replicas from the pulse replicator versus the relative angle of the two reflectors of the OPR. The value of α minimizing the spread of the relative positions is indicated by a white dashed line. (b) Nonlinear component of the delay for 50 replicas from the pulse replicator for the relative angle minimizing the standard deviation of the relative positions.

Experimental Results

1. Experimental Setup

A prototype single-shot cross-correlator was built with 2-in. reflectors. The off-the-shelf commercial reflectors have a surface figure of $\lambda/10$ at 633 nm. The partial reflector has $R = 99\%$ at 0°. The angle between the input beam and the reflectors is approximately 20°. The layout is similar to that of Fig. 114.36(a), with a metal mirror between the beam combiner and the THG crystal folding the 1ω and 2ω beam paths to reduce the footprint of the device. The horizontal width of the 2ω beam before replication was reduced by using a telescope to increase the number of replicas produced by the replicator. The distance Z between the OPR and nonlinear crystal is 130 cm. The nonlinear crystal is a 5-mm, type-II DKDP cut for THG ($\theta \sim 59°$). The polarizations of the 1ω and 2ω beams are vertical and horizontal, respectively, and the crystal is oriented accordingly. The angular spread of the 2ω beams after the replicator is in the horizontal direction, which is aligned with the ordinary axis of the crystal to decrease the phase-matching angular variation. The 1ω and 2ω beams are multiplexed vertically with a small angle so that they overlap in the THG crystal.

Optical pulses from a diode-pumped regenerative amplifier (DPRA) operating at 1053 nm were used to demonstrate the single-shot, high-dynamic-range cross-correlator. The DPRA is seeded by a short optical pulse (sub-200 fs) from a mode-locked laser. After amplification and gain narrowing, the amplifier delivers an ~8-ps pulse at 5 Hz with an energy per pulse of approximately 250 μJ. Second-harmonic generation is performed in a 10-mm, type-I lithium triborate (LBO) crystal. The 2ω energy before the replicator is 60 μJ. With the 5-mm DKDP crystal, the noise-equivalent input 1ω energy of the contrast diagnostic is approximately 7 pJ. The sampling pulses need not be derived from the pulse under test, and a low-energy pulse under test could be characterized using sampling pulses generated by another source.

The THG signal is measured with a video camera connected to a frame grabber. The 1ω and 2ω sources are blocked before detection with colored filters. The dynamic range of the diagnostic using this eight-bit frame grabber was determined by measuring the signal corresponding to a single 3ω replica versus input 1ω energy. For a spatially extended 3ω beam, the dynamic range is higher than at each point in the beam because lower-intensity parts of the beam can linearly contribute to the signal even when other parts are saturated. A dynamic range of the order of 30 dB was obtained (Fig. 114.39). Additionally, the 3ω signal versus input 1ω energy was measured when a

E16623JRC

E16624JRC
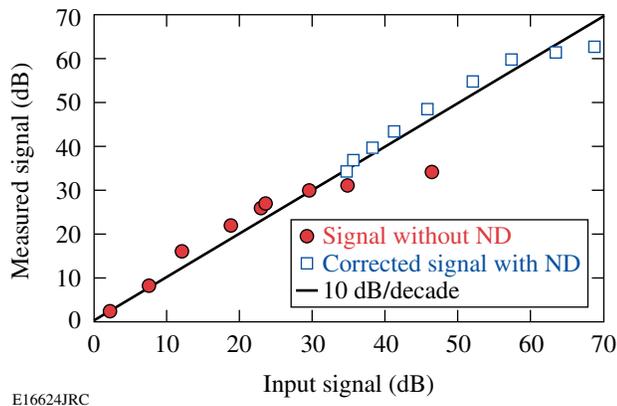
Figure 114.39
Measured 3ω signal versus 1ω signal without neutral-density (ND) filters on the sampling pulse (circles) and with a 30-dB attenuation on the sampling pulse after signal correction (squares). The solid line corresponds to the expected linear relation between the input and output signals.

neutral-density filter with an optical density of 3 was set in front of the 2ω replicas used for up-conversion. As expected from the THG process, the THG signal decreases by three orders of magnitude for the same input 1ω energy, and a 30-dB decrease in the 2ω sampling energy is compensated by a 30-dB increase in 1ω energy. This demonstrates the potential enhancement of the dynamic range of the diagnostic using density filters on specific sampling pulses that are known to correspond to high-intensity portions of the pulse under test. Thanks to the discrete spatial-intensity distribution of the sampling pulses, attenuation can be performed with off-the-shelf density filters. Attenuation of the sampling source, as opposed to the attenuation of the signal after interaction,[9] was chosen to minimize scattering. Scattering of the sampling pulses at a non-detected wavelength before the nonlinear interaction is preferred over scattering of a high-intensity signal at the detected wavelength after the nonlinear interaction to preserve the high dynamic range of the diagnostic.

The sampling rate was calibrated by temporally scanning the 1ω pulse relative to the train of sampling pulses. The variations of the 3ω signal intensity in each time slot were calibrated using this scan to correct the measured signals. These variations potentially arise from the non-identical spatial overlap of the sampling pulses with the 1ω pulse in the crystal, from the 2ω energy-per-replica variation at the output of the OPR, and from the phase-matching variations in the tripling crystal among different 2ω pulses arriving at different angles.

2. Measurement of a Train of Pulses from a Fabry–Perot Etalon

The intensity and temporal calibration of the diagnostic were tested by inserting a Fabry–Perot etalon in the 1ω optical beam path. The etalon generates a sequence of optical pulses separated by the intracavity round-trip time, 40 ps in this case. Figure 114.40 shows the intensity histogram measured over 1000 shots, which is similar to the infinite-persistence mode of sampling oscilloscopes. Five pulses from the pulse train are well resolved by the diagnostic. As expected, the separation between pulses is approximately 40 ps, and their intensity decreases monotonically. Energy fluctuations from the DPRA can also be seen.

E16625JR
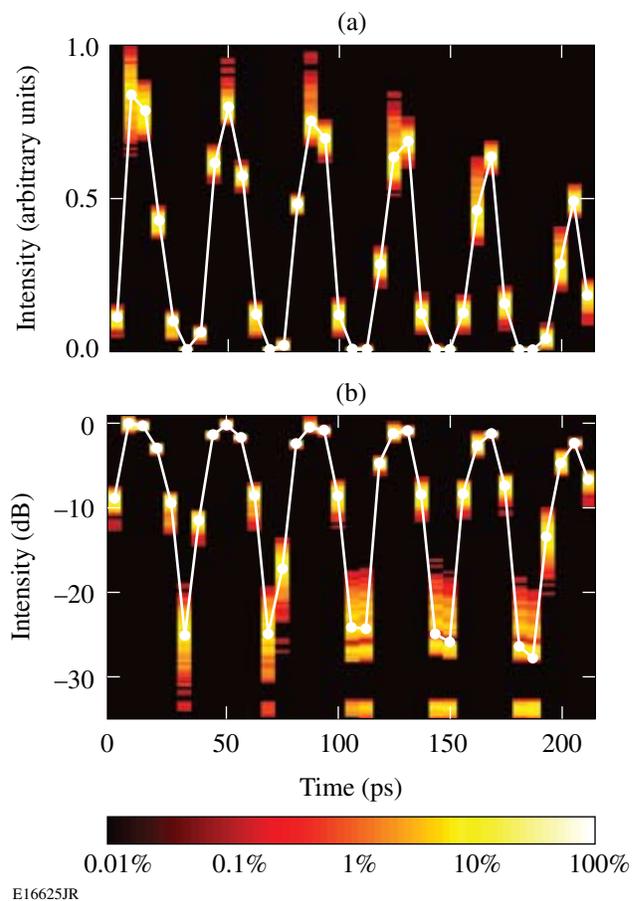
Figure 114.40
Intensity histogram of the output of a Fabry–Perot etalon on (a) a linear scale and (b) logarithmic scale. In each case, the average value of the intensity at each time slot is plotted with white circles.

3. High-Dynamic-Range Measurements

Figure 114.41 demonstrates the high dynamic range of the diagnostic. The sensitivity of the device was adapted to measure

the prepulse contrast. A neutral-density filter with an optical density of 3 at 2ω was set at the output of the pulse replicator to attenuate the seven last sampling pulses, which were timed to coincide with the main pulse from the DPRA. This effectively allows one to map the signal intensity over more than 60 dB onto the detector. The intensity histogram of 10,000 successive shots of the DPRA shows the presence of a prepulse approximately 100 ps before and 40 dB below the main pulse. Amplified spontaneous emission (ASE) has an average intensity approximately 45 dB below the peak intensity of the pulse, although there are large shot-to-shot intensity variations due to the incoherent nature of ASE. Figure 114.42(a) shows the intensity of one DPRA shot, while Fig. 114.42(b) shows the intensity averaged over 10,000 shots.
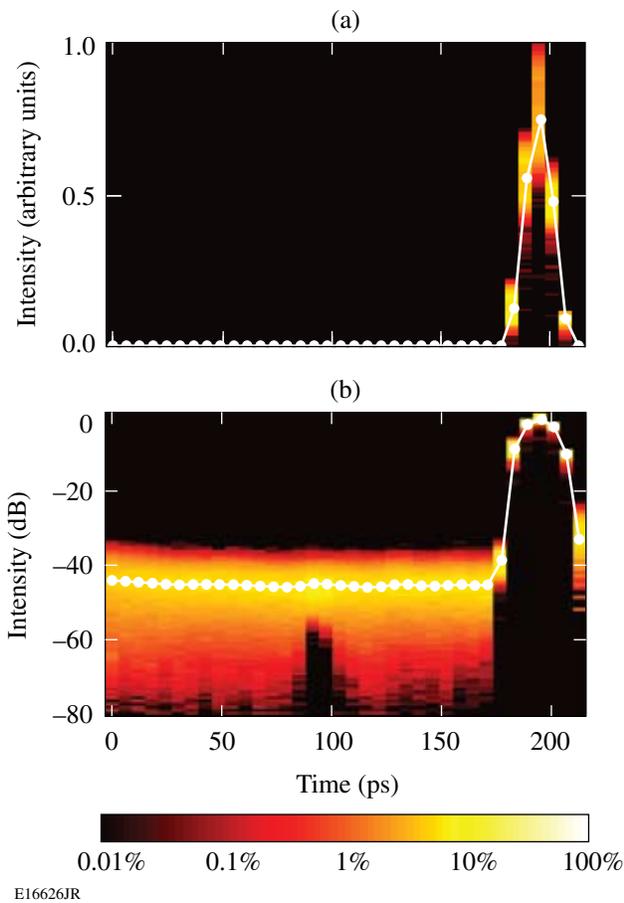
Figure 114.41
Intensity histogram of 10,000 successive shots of the DPRA on (a) linear and (b) logarithmic scales. In each time slot, brighter intensity corresponds to a larger proportion of samples in a given intensity bin. The average intensity is plotted with white circles. A prepulse can be observed approximately 100 ps before the main pulse.
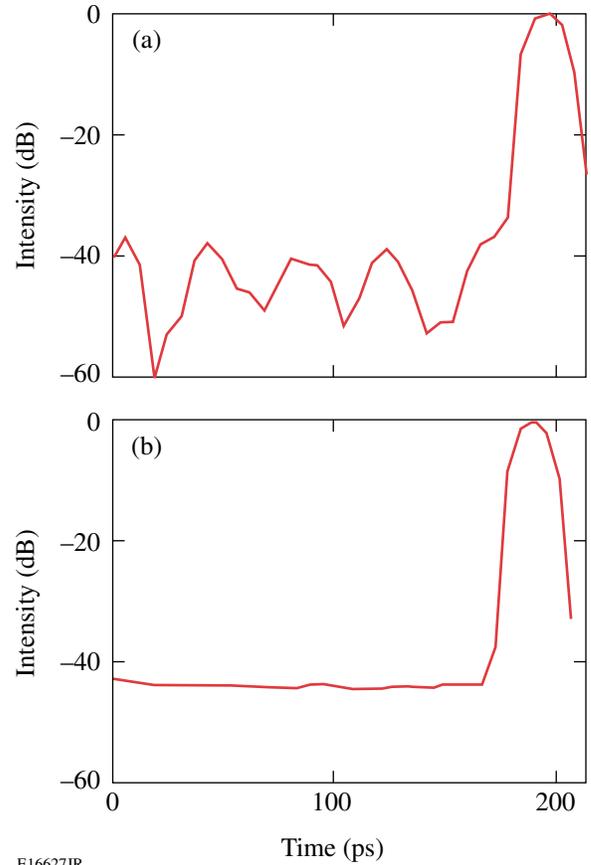
Figure 114.42
(a) Intensity of one DPRA shot and (b) intensity averaged over 10,000 shots.

4. Measurement of Amplified Spontaneous Emission

ASE is a time-stationary incoherent process, and one expects that its statistical temporal properties do not depend on time. The observation window of the cross-correlator was moved significantly in front of the pulse from the DPRA. Figure 114.43 shows the histogram of the measured intensity, with the average value plotted with white circles. Very uniform distribution of the intensity samples can be observed on the linear and logarithmic plots.

5. Statistical Analysis

Incoherent laser and parametric fluorescence are commonly present on high-energy laser pulses. The statistical properties of the intensity of ASE are well documented.[12] For ASE with a degree of polarization equal to 1 (i.e., linearly polarized ASE), the intensity probability density is

$$P(I) = \frac{1}{\langle I \rangle} \exp\left(-\frac{I}{\langle I \rangle}\right), \tag{5}$$
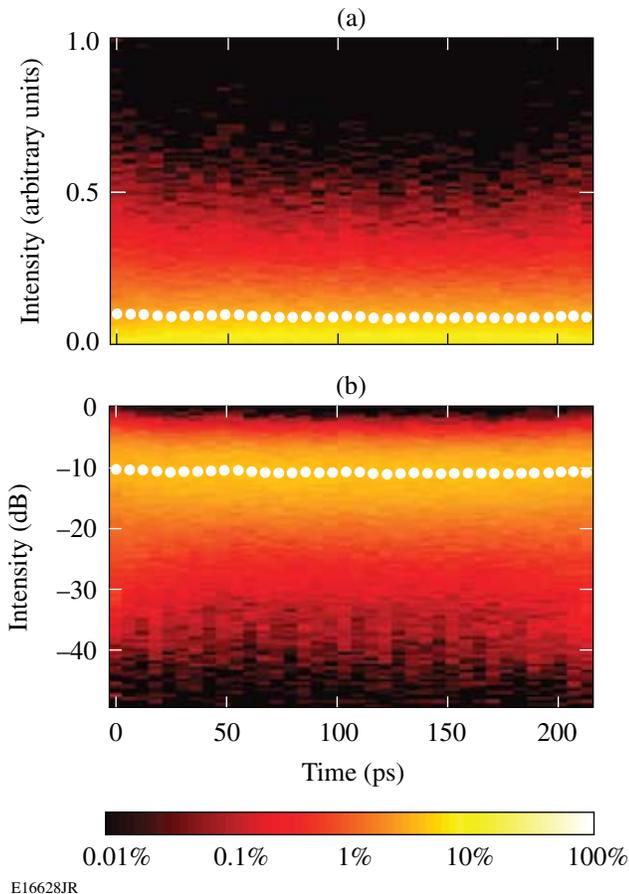
Figure 114.43
Intensity histogram of 10,000 realizations of ASE on (a) linear and (b) logarithmic scales. In each case, the average value of the intensity at each time slot is plotted with white circles.

Figure 114.44
Intensity probability density distribution for amplified spontaneous emission. Plots (a) and (c) correspond to an overlap of the distributions obtained at each of the 36 time slots characterized by the diagnostic on a linear and logarithmic scale, respectively. Plots (b) and (d) correspond to the distribution calculated with all the measured samples on a linear and logarithmic scale, respectively. Experimental distributions are plotted with thin solid lines, and the theoretical prediction of Eq. (5) is plotted with circles.

where $\langle I \rangle$ is the average value of the intensity. Equation (5) is remarkable since it does not rely on any free parameter. A collection of samples of the intensity of an incoherent process should match this distribution and confirm that the measured variations are indeed on the signal under test and are not due to the diagnostic. Figure 114.44(a) shows the measured intensity probability distributions at each of the 36 measured time slots (i.e., 36 different probability density distributions are calculated, each of them using the 10,000 intensity samples measured at a given time). An excellent overlap of the distributions and a good agreement with the expected distribution of Eq. (5) are obtained. Figure 114.44(b) corresponds to the measured intensity probability distribution when all the collected samples (i.e., 36,000 samples) are considered as a single set. An excellent agreement with the expected distribution is again obtained. Figures 114.44(c) and 114.44(d) are logarithmic representations of the data plotted in Figs. 114.44(a) and 114.44(b), respectively. They reinforce the property that accurate intensity measurements are performed over a 30-dB dynamic range.

Figure 114.45 displays the normalized quantity $\sigma_N(I) = \sigma(I)/\langle I \rangle$ for the data from Figs. 114.41 and 114.43. For the incoherent process described by Eq. (5), one expects $\sigma_N(I) = 1$. Values slightly higher than 1 are measured, with a slightly increased value at the edges of the measurement range [Fig. 114.45(a)]. Higher noise is attributed to photodetection noise. In these measurements, the signal corresponding to the outer replicas before intensity calibration is lower, and the relative detection noise would be higher. For a coherent process, it is expected that $\sigma_N(I) = 0$, while for a combination of a coherent and incoherent process, all values of $\sigma_N(I)$ between 0 and 1 are achievable. Figure 114.45(b) displays $\sigma_N(I)$ for the data in Fig. 114.41. This quantity is very close to 0 at times corresponding to the main pulse. It is essentially identical to its values in Fig. 114.45(a) at times corresponding to ASE only. The small prepulse approximately 100 ps before the main pulse corresponds to an observable decrease of $\sigma_N(I)$. While the noise at
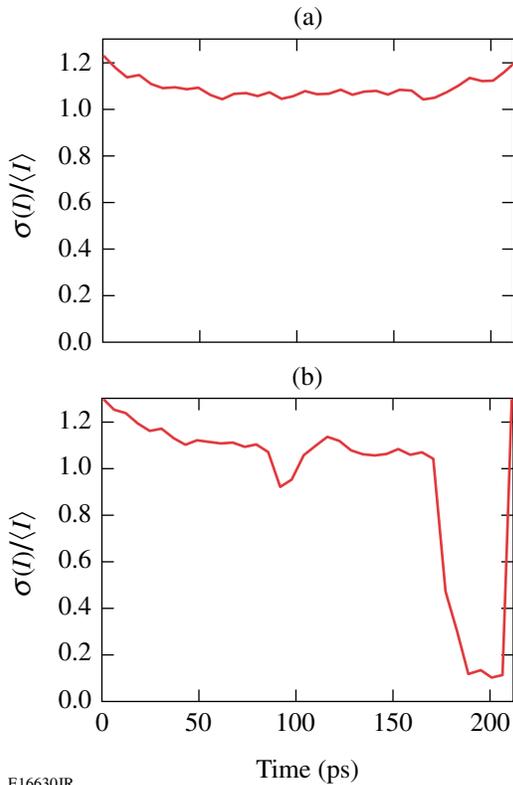
Figure 114.45
Normalized intensity standard deviation as a function of time for amplified spontaneous emission (in relation to Fig. 114.43) and for a 200-ps window including the main laser pulse (in relation to Fig. 114.41).

these times is small relative to the main pulse, it is significant relative to the intensity of the prepulse.

Conclusion

A single-shot cross-correlator based on a discrete sequence of sampling optical pulses has been demonstrated. Versatile operation has allowed the characterization of different optical sources. The demonstrated high dynamic range (60 dB) and large temporal coverage (200 ps) make this temporal diagnostic a valuable tool to measure the temporal contrast of optical pulses. The capabilities of this cross-correlator can be extended in various directions. The temporal range can be directly increased by using larger reflectors in the optical pulse replicator. The temporal dynamic range can be improved by increasing the dynamic range of the spatial-intensity measurement of the gated signal. For example, additional optical densities can be used after the pulse replicator to characterize optical sources with higher contrast requirements.

REFERENCES

1. S.-W. Bahk, P. Rousseau, T. A. Planchon, V. Chvykov, G. Kalintchenko, A. Maksimchuk, G. A. Mourou, and V. Yanovksy, Opt. Lett. **29**, 2837 (2004).

2. J. D. Zuegel, S. Borneis, C. Barty, B. LeGarrec, C. Danson, N. Miyanaga, P. K. Rambo, C. LeBlanc, T. J. Kessler, A. W. Schmid, L. J. Waxer, J. H. Kelly, B. Kruschwitz, R. Jungquist, E. Moses, J. Britten, I. Jovanovic, J. Dawson, and N. Blanchot, Fusion Sci. Technol. **49**, 453 (2006).

3. D. J. Kane and R. Trebino, Opt. Lett. **18**, 823 (1993).

4. C. Dorrer, B. de Beauvoir, C. Le Blanc, S. Ranc, J.-P. Rousseau, P. Rousseau, and J.-P. Chambaret, Opt. Lett. **24**, 1644 (1999).

5. J. Bromage, C. Dorrer, I. A. Begishev, N. G. Usechak, and J. D. Zuegel, Opt. Lett. **31**, 3523 (2006).

6. S. Luan *et al.*, Meas. Sci. Technol. **4**, 1426 (1993).

7. E. J. Divall and I. N. Ross, Opt. Lett. **29**, 2273 (2004).

8. J. Collier *et al.*, Laser Part. Beams **19**, 231 (2001).

9. I. Jovanovic *et al.*, presented at the CLEO/QELS Conference, Baltimore, MD, 6–11 May 2007 (Paper JThD137).

10. C. Dufour, Rev. Opt. **24**, 11 (1945).

11. S. Xiao, J. D. McKinney, and A. M. Weiner, IEEE Photonics Technol. Lett. **16**, 1936 (2004).

12. L. Mandel and E. Wolf, *Optical Coherence and Quantum Optics* (Cambridge University Press, Cambridge, England, 1995).

E16630JR